Physica E 124 (2020) 114352

Contents lists available at ScienceDirect

Physica E: Low-dimensional Systems and Nanostructures

journal homepage: http://www.elsevier.com/locate/physe

The effect of microstructural features on the ferromagnetism of nickel oxide nanoparticles synthesized in a low-pressure arc plasma

A.V. Ushakov [a,b], I.V. Karpov [a,b], L.Yu. Fedorov [a,b,*], V.G. Demin [b], E.A. Goncharova [b], A. A. Shaihadinov [b], G.M. Zeer [b], S.M. Zharkov [b,c]

[a] Federal Research Center "Krasnoyarsk Scientific Center", Siberian Branch of the Russian Academy of Sciences, 660036, Krasnoyarsk, Russia
[b] Siberian Federal University, Krasnoyarsk, 660041, Russia
[c] Kirensky Institute of Physics, Federal Research Center "Krasnoyarsk Scientific Center", Siberian Branch, Russian Academy of Sciences, 660036, Krasnoyarsk, Russia

ARTICLE INFO

Keywords:
Nickel oxide
Nanoparticles
Band gap
Magnetic properties

ABSTRACT

Nickel oxide nanoparticles were first synthesized by sputtering high-purity nickel in an oxygen plasma of a low-pressure arc discharge. The structure, morphology, and optical and magnetic properties of NiO nanoparticles were studied by XRD, TEM, FTIR, UV-VIS, and VSM. TEM images showed that the obtained NiO nanoparticles have a narrow particle size distribution and an average particle size of 12 nm. The XRD results and the processing of diffractograms by the Rietveld method showed that the obtained nanoparticles have a face-centered cubic lattice with an average particle size of 13 nm. With decreasing temperature, residual stresses increase and peaks corresponding to the superstructure appear. The band gap of NiO was determined from the optical absorption spectrum and amounted to 3.21 eV. Magnetic measurements showed that, at temperatures of 200 and 300 K, NiO nanoparticles, unlike bulk particles, exhibit ferromagnetic behavior, and at 5 K a magnetic hysteresis loop appears. Based on the studies, a dendritic model of the nanoparticle microstructure is proposed.

1. Introduction

Currently, interest is increasing in magnetic nanoparticles exhibiting unusual electrophysical, chemical, and optical properties, which is associated with the manifestation of the so-called "quantum size effects" [1–4]. Of greatest interest are magnetic nanoparticles with antiferromagnetic ordering, which are widely used as magnetic memory devices, recording audio and video signals, for example, magnetic tapes, hard drives, etc. The most popular are antiferromagnets based on transition metal oxides (NiO, CuO, MnO, etc.) [5–9]. Coarse-grained nickel oxide is an antiferromagnet with a Neel temperature of 523 K. In the nanodispersed state of NiO, due to the fact that the fraction of surface atoms increases, the number of defects, elastic stresses increases, and it exhibits various types of magnetic ordering [10–13]. We observed the presence of superparamagnetic or ferromagnetic behavior of NiO nanoparticles with a particle size in the range of 2–6 Nm, ferromagnetic behavior with narrow hysteresis loops and coercivity of about 750 Oe at 5 K. Thanks to this, nanodispersed NiO can be claimed in various magnetic memory devices.

To obtain nickel oxide nanoparticles, various physicochemical methods are used, such as sol-gel, chemical deposition, microwave method, plasma-chemical methods [12,14–19]. The plasma-chemical method in a plasma of a low-pressure arc discharge has shown its high efficiency in the synthesis of copper oxide nanoparticles [20–22]. Nanoparticles with an average size of less than 10 nm were obtained. The method is characterized by high productivity, the ability to obtain complex chemical compounds in plasma. Allows you to control the size of the nanoparticles, residual stresses, stoichiometry and phase composition. The obtained nanoparticles of copper oxide, depending on the temperature and intensity of the external magnetic field, show a wide variety of magnetic properties. In the region of low field strength, the ferromagnetic state dominates over the entire temperature range under study, at high field strengths and temperatures below 200 K, the paramagnetic state prevails, at high field strengths (more than 3 kOe) and temperatures above 300 K, the diamagnetic state of nanoparticles is switched on [23]. In this case, the temperature of antiferromagnetic ordering decreases significantly (to ~ 100 K).

This work is aimed at linking the morphological and microstructural

* Corresponding author. Federal Research Center "Krasnoyarsk Scientific Center", Siberian Branch of the Russian Academy of Sciences, 660036, Krasnoyarsk, Russia.
E-mail address: sfu-unesco@mail.ru (L.Yu. Fedorov).

https://doi.org/10.1016/j.physe.2020.114352
Received 12 February 2020; Received in revised form 2 July 2020; Accepted 4 July 2020
Available online 10 July 2020

features of nickel oxide nanoparticles obtained under conditions of high-speed plasma-chemical synthesis in a low-pressure arc discharge plasma with their anomalous magnetic properties.

2. Experimental

The technological features of the synthesis of nanopowders in a plasma of a low-pressure arc discharge, as well as the experimental setup, are described in detail in [20–22]. For the synthesis of nickel oxide nanopowder, a high-purity cathode (99.9%) was used. The cathode was evaporated in a gas mixture of argon and oxygen at a pressure of 80 Pa, while direct plasma-chemical synthesis of nickel oxide nanoparticles occurred. The supply of plasma-forming gas, oxygen and the geometry of the arc evaporator are optimized in such a way as to avoid the appearance of a microdrop fraction and to provide plasma-chemical synthesis. Using a JEOL JEM-2100 transmission electron microscope, the morphological features of the samples were studied. The phase composition was studied in the temperature range from 100 to 300 K using a Bruker AXS D8 Advance X-ray diffractometer in CuK_α monochromatized radiation with a low-temperature (TTK450) attachment. To identify XRD spectra, the PDF4 + database was used. Quantitative structural-phase analysis of diffraction patterns was carried out using the Powder Cell 2.4 full-profile analysis program. The UV–visible spectra of NiO nanoparticles were measured using a USB-2000 UV–Vis spectrophotometer. IR spectra were analyzed on a Nicolet 6700 IR Fourier spectrometer with a resolution of up to 0.09 cm^{-1} in the spectral range 25,000-20 cm^{-1}. Magnetic measurements were carried out using a SQUID magnetometer (Quantum Design).

3. Results and discussion

Fig. 1 shows the TEM image, histograms, and size distribution functions of the size of NiO nanoparticles obtained in an arc discharge plasma at a gas mixture pressure of 90% Ar + 10% O_2 80 Pa.

In the TEM image, it is seen that the obtained nanoparticles have an almost spherical shape and are strongly agglomerated, which is typical for plasma-chemical synthesis nanoparticles. As previously emphasized [20–22], nanoparticles have high surface energy.

The crystalline ordering of particles with a large (about 2 nm) lattice parameter is clearly visible in the image. The mathematical processing of the obtained images by the secant method showed that the particle sizes vary in the range from 5 to 25 nm. Histograms were built and the data obtained were processed. The average nanoparticle size was 12 nm. Particles are characterized by both normal and lognormal particle size distributions. Based on the presented distribution function, the condensation process is carried out from the cluster and vapor phases, respectively. However, the coagulation process is most likely for plasmachemical synthesis. This mechanism is characterized by the collision of clusters and particles of various sizes and their coalescence, recrystallization, coalescence.

In Fig. 2 shows the XRD spectra of NiO nanoparticles obtained at different temperatures. Above the Néel temperature (523 K), NiO is paramagnetic and has a cubic crystal lattice with space group Fm-3m and lattice parameter a = 4.1677 Å. At low temperatures, NiO exhibits antiferromagnetic properties. In this case, the crystal lattice exhibits trigonal/rhombohedral distortion (space group *R-3mH*).

Over the entire temperature range, the peaks in the XRD spectrum of the NiO sample correspond to a face-centered cubic lattice (*FCC* phase) with the parameter a = 4.194 Å according to JCPDS No. 89-7130. The entire XRD spectrum of NiO samples shows standard peaks at 37 deg, 43 deg, 63 deg, 75 deg and 79 deg corresponding to the (111), (200), (220), (311) and (222) planes, respectively. The average size of the coherent scattering regions (CSR) and residual stresses were calculated using the Debye-Scherrer formula using the Powder Cell 2.4 full-profile analysis program. The average CSR size of NiO nanoparticles in the entire temperature range was 13 nm, which is in good agreement with microscopic studies. With decreasing temperature, the residual stresses increase: −510 MPa at 200 K, −580 MPa at 100 K. At a temperature of 200 K, peaks (marked by arrows) corresponding to a monoclinic (space group *C2/m* (*A12/m1*)) superstructure become noticeable with the base lattice period a = 4.0527 Å.

In Fig. 3 shows the FTIR spectrum of NiO nanoparticles obtained at a gas mixture pressure of 90% Ar + 10% O_2 in a 80 Pa plasma chemical

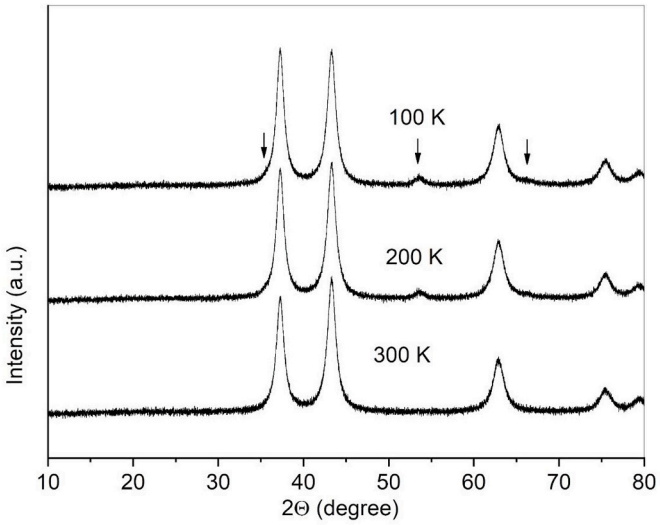

Fig. 2. XRD спектр of particles NiO obtained in arc discharge plasma at a gas mixture 90% Ar + 10% O_2 80 Pa.

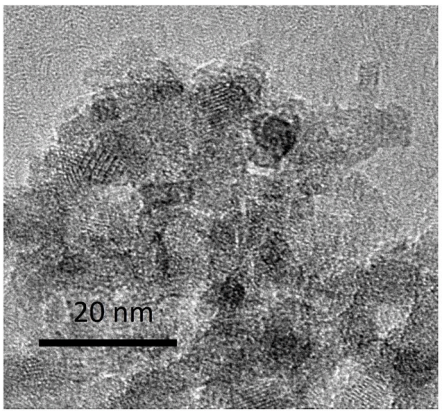

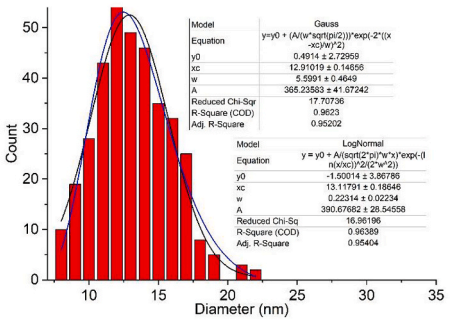

Fig. 1. TEM image histograms and size distribution functions of particles NiO obtained in arc discharge plasma at a gas mixture 90% Ar + 10% O_2 80 Pa.

reactor. The absorption frequencies due to interatomic vibrations in metal oxides are shifted to a region below 1000 cm^{-1}. In the FTIR spectrum, the peak of the absorption band of 431 cm^{-1} is responsible for the vibrational mode of the Ni atom. The three peaks of 522, 1115, and 1162 cm^{-1}, characteristic of Ni (II) –O and Ni–O–H, are responsible for symmetric and asymmetric frequencies. The similarity of the IR spectra of the nanoparticles is explained by small particle sizes, which is confirmed by XRD studies.

The absorption bands arising between 827 and 1153 cm^{-1} can be attributed to the symmetric and asymmetric stretching modes O–C = O and the stretching vibrations C–O. The band at 1619 cm^{-1} refers to the H–O–H vibration band, which indicates that NiO nanoparticles contain crystalline water. The band at 1113 cm^{-1} indicates the C–O–Ni extension of nanoparticles. The high specific surface of the nanoparticles leads to enhanced absorption of atmospheric moisture and the appearance of vibrations of bound OH groups, which is reflected in the spectrum as a wide absorption band with a peak at 3414 cm^{-1}. The appearance of the absorption band at 1622–1383 cm^{-1} can be related by the deformation vibrations of the residual water δ (HOH).

Fig. 4 shows the optical absorption spectra for NiO nanoparticles. The resulting NiO nanoparticles exhibit strong absorption in the UV region. The observed characteristic absorption peak is located at 307 nm. Such absorption in the UV region appears due to direct transitions of the forbidden band of NiO nanostructures. The band gap of NiO nanoparticles can be determined using the optical absorption spectrum using the following Tauc equation [24]:

$$(\alpha h\upsilon)^{n} = B\left(h\upsilon - E_g\right)$$

where α, hν, *B* is the absorption coefficient, photon energy, and the constant associated with the material, respectively, n = 2 for the direct transition. Extrapolation of the dependence of $(\alpha h\nu)^2$ on $h\nu$ gives the band gap of NiO. The band gap for NiO nanoparticles was 3.21 eV, which is significantly lower than 4.0 eV for bulk NiO. The reduced band gap for NiO nanoparticles and the blue shift of the absorption region are due to the quantum-size effect in the nanoscale region [25].

Fig. 5 shows the isothermal dependences of the magnetization *M* on the magnetic field strength. As follows from the figure, for the obtained NiO nanoparticles, the shape of the curves is characteristic of superparamagnetic or antiferromagnetic materials with a ferromagnetic impurity. However, fitting does not support these assumptions. The magnetization of superparamagnets as a function of magnetic induction and temperature is well described by the modified Langevin function

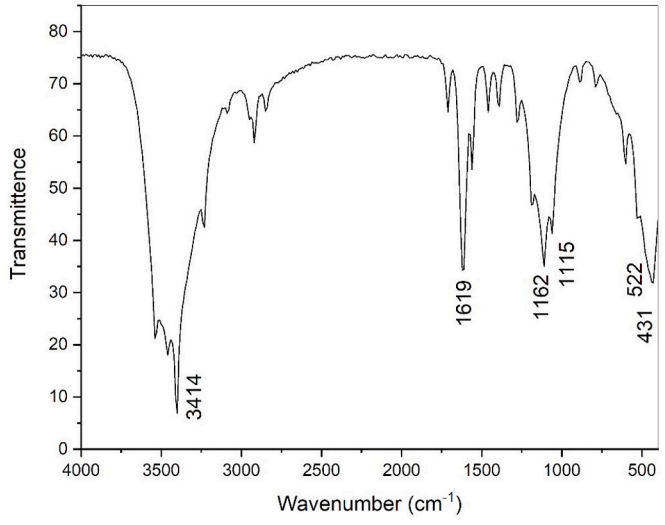

Fig. 3. FTIR spectrum of a NiO nanopowder obtained in a plasma arc discharge at a gas mixture pressure of 90% Ar + 10% O_2 80 Pa.

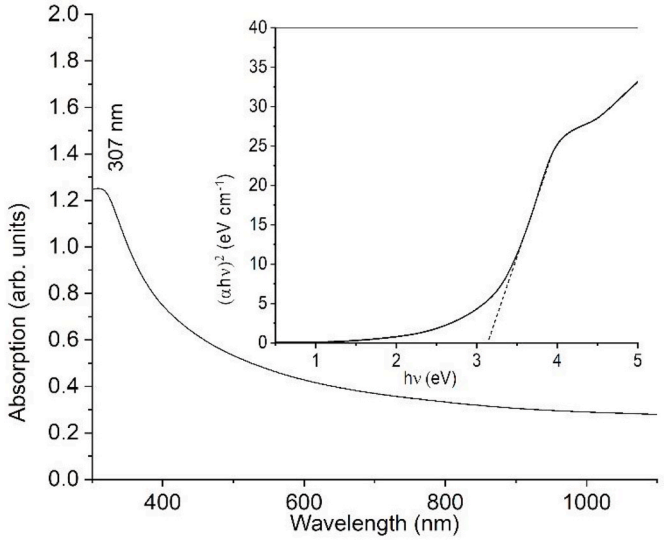

Fig. 4. Optical absorption and band gap curve (inset) for nanoparticles obtained in an arc discharge plasma at a gas mixture pressure of 90% Ar + 10% O_2 80 Pa.

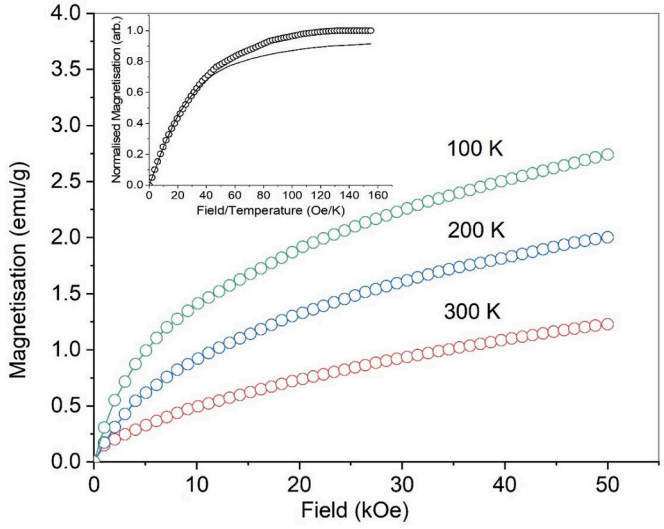

Fig. 5. *M*(*H*) dependences of NiO nanoparticles at the indicated temperatures, inset shows the 300 K curve fitted with a Langevin curve.

[26]: $M = M_0L(x) + \chi_a B$. $\chi_a B$ describes the canting of the AF sublattices of the particle cores, $L(x) = \coth(x) - \frac{1}{x}$ is the Langevin function, the argument of the function $x = \frac{(\mu_p B)}{(k_B T)}$, k_B is the Boltzmann constant, the fitting parameters: M_0 is the saturation magnetization, χ_a is the magnetic susceptibility of the randomly oriented AF particle cores, and μ_p is the magnetic moment of the particle. When fitting, it is necessary to take into account the relationship between the parameters $M_0 \tilde{} N \cdot \mu_p$, where *N* is the specific number of particles. The results of data fitting for the normalized magnetization curve at 300 K are shown in the inset. As can be seen from the graph, even at temperatures above T_B, the behavior of the magnetization curve does not coincide with the prediction of the theory of superparamagnetism. At temperatures below T_B, the deviation is even greater. It can be assumed that there is a complex interaction of the magnetic field with the antiferromagnetic core and the spin-glass shell of the nanoparticles. In addition, it is necessary to take into account the anisotropy of the shell shape and the magnetoelastic anisotropy of the nucleus due to residual stresses arising in the

nanoparticle during high-speed plasma-chemical synthesis.

With decreasing temperature, the contribution to the magnetization from the bulk and shell anisotropy sharply increases and we can speak of a new magnetic state. Fig. 6 shows the isothermal dependences of the magnetization in the FC and ZFC modes at a temperature of 5 K. The coercive forces of the hysteresis loops are approximately equal and amount to 420 Oe. The residual magnetization in FC mode was 0.98 emu/g, while for ZFC it was slightly less - 0.76 emu/g. No exchange bias or any features in coercivity were found. However, the nature of the shell ferromagnetism may be different and traditional approaches to exchange bias may not be applicable. It should be noted that there is a significant jump in the magnetic moment associated with phase transitions with decreasing temperature, or with the competition of various anisotropies in the nanoparticle. The complex exchange interaction of the ferromagnetic shell with the antiferromagnetic core is reflected in the dependence $M(T)$ in a constant magnetic field of 1 kOe, which is presented in the tab in Fig. 6.

Three characteristic points can be determined on the $M_{ZFC}(T)$ curves that determine the nature of the interaction with the magnetic field: a sharp peak at a freezing temperature $T_f \sim 7$ K, a wide maximum at a blocking temperature $T_B \sim 146$ K, and a splitting temperature $T_{irr} \sim 280$ K. into the core-shell model [27,28]. In the process of condensation on the substrate, the nanoparticle grows from the vapor phase and then oxidizes due to oxygen plasma. Since the speed of the plasma-chemical process is high, the nanoparticle is formed with oxygen vacancies. In this case, the AFM core is formed with uncompensated magnetic sublattices, creating a magnetic moment. The magnetically chaotic shell thermally behaves like a spin-glass system. In such a model, above a certain temperature, the core will exhibit superparamagnetic properties. However, as shown in Fig. 5, this does not happen.

According to Fig. 1, nanoparticles have a particle size distribution that correlates with the distribution of energy barriers and, accordingly, the magnetic moments of the nanoparticles are blocked in a certain temperature range. The obtained value of T_f can be interpreted as the freezing temperature of the shell spins. This process can be associated with the competing interaction of cubic and uniaxial anisotropy. As was shown in [29], magnetic phenomena in plasma chemical synthesis nanopowders are directly related to the coagulation process of nanoparticle growth from the cluster phase, as shown in Fig. 1. Since the crystallization process is avalanche-like, the nanoparticles have a dendritic structure with a predominant growth towards the evaporator. Uniaxial magnetic anisotropy can be associated precisely with the dendritic structure of nanoparticles. The diameter of an individual dendrite reaches a cluster size of ~2 nm. Such structures are clearly visible on the XRD spectra in the form of broadening of the base of peaks or halo. Oxygen stoichiometry can also vary widely from deficit to excess, depending on the thermal state of the substrate. In this case, the nanoparticles experience significant structural deformation due to the high surface energy. As the full-profile processing of XRD spectral lines by the Rietveld method shows, line broadening is associated with significant crystal deformation, and the appearance of superstructural peaks with decreasing temperature confirms the assumption of oxygen vacancies and the coagulation process. The relationship between magnetoelastic anisotropy and ferromagnetism in nanowires was studied in [30,31]. In our case, the appearance of hysteresis loops (Fig. 6) can also be associated with residual deformation in nanoparticles, due to which the exchange bonds between nickel ions are strengthened and the long-range magnetic order appears. The dendritic model of the nanoparticle microstructure explains the behavior of the $M_{ZFC}(B)$ dependence curve at freezing temperature (inset in Fig. 6) and the lack of a clear effect (inset in Fig. 6) of exchange anisotropy at the interface between the core and the shell, since the transition is smooth.

4. Conclusion

Studies have shown that the method of synthesis of nanoparticles in oxygen plasma of a low-pressure arc discharge is an effective tool for the synthesis of monophasic nanocrystalline NiO particles. X-ray diffraction analysis shows that the prepared sample is in a cubic phase. The wide peak of the X-ray diffraction pattern indicates the nanocrystalline behavior of the particles. TEM images confirm that NiO nanoparticles are spherical in nanoscale. The study of the magnetic properties of the samples using the VSM method shows that NiO nanoparticles exhibit complex magnetic behavior depending on the magnetic field strength and temperature. All the results obtained indicate that NiO nanoparticles have a really noticeable magnetic response and are a suitable magnetic material for recording devices.

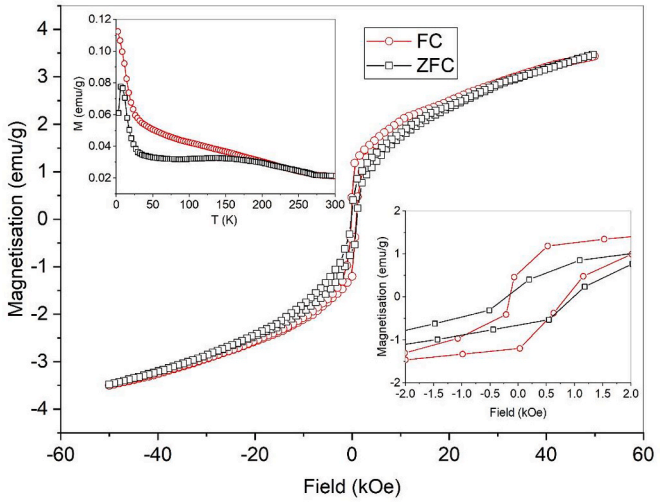

Fig. 6. Hysteresis loops depending on the magnetization of NiO nanoparticles on the applied field in the FC (red) and ZFC (black) modes. The insets show enlarged hysteresis loops and $M(T)$ curves in FC and ZFC modes. (For interpretation of the references to colour in this figure legend, the reader is referred to the Web version of this article.)

Declaration of competing interest

The authors declare that they have no known competing financial interests or personal relationships that could have appeared to influence the work reported in this paper.

CRediT authorship contribution statement

A.V. Ushakov: Conceptualization, Writing - original draft. **I.V. Karpov:** Methodology, Writing - review & editing. **L.Yu. Fedorov:** Resources, Investigation. **V.G. Demin:** Investigation. **E.A. Goncharova:** Visualization. **A.A. Shaihadinov:** Investigation. **G.M. Zeer:** Resources. **S.M. Zharkov:** Resources.

Acknowledgements

The work was performed with a support of the grant of the Russian Science Foundation (Project No. 16-19-10054). The electron microscopy investigations were conducted in the SFU Joint Scientific Center supported by the State assignment (#FSRZ-2020-0011) of the Ministry of Science and Higher Education of the Russian Federation.

List of acronyms and abbreviations

XRD	X-Ray diffraction
TEM	transmission electron microscopy
FTIR	Fourier-transform infrared spectroscopy
UV-VIS	ultraviolet–visible spectroscopy
VSM	vibrating sample magnetometer

SQUID	superconducting quantum interference device
IR	infrared
CSR	coherent scattering regions
AF	antiferromagnetic
FC	field cooled
ZFC	zero field cooled

References

[1] D. Lisjak, A. Mertelj, Anisotropic magnetic nanoparticles: a review of their properties, syntheses and potential applications, Prog. Mater. Sci. 95 (2018) 286–328, https://doi.org/10.1016/j.pmatsci.2018.03.003.

[2] X. Fuku, N. Matinise, M. Masikini, K. Kasinathan, M. Maaza, An electrochemically active green synthesized polycrystalline NiO/MgO catalyst: use in photo-catalytic applications, Mat. Res. Bull. 97 (2018) 457–465, https://doi.org/10.1016/j.materresbull.2017.09.022.

[3] A. Kumar Rai, L. Tuan Anh, C.-J. Park, J. Kim, Electrochemical study of NiO nanoparticles electrode for application in rechargeable lithium-ion batteries, Ceramics Int. 39 (6) (2013) 6611–6618, https://doi.org/10.1016/j.ceramint.2013.01.097.

[4] R.M. Silva, R.A. Raimundo, W.V. Fernandes, S.M. Torres, V.D. Silva, J.P.F. Grilo, M.A. Morales, D.A. Macedo, Proteic sol-gel synthesis, structure and magnetic properties of Ni/NiO core-shell powders, Ceramics Int. 44 (6) (2018) 6152–6156, https://doi.org/10.1016/j.ceramint.2017.12.248.

[5] Y. Bi, A. Nautiyal, H. Zhang, J. Luo, X. Zhang, One-pot microwave synthesis of NiO/MnO_2 composite as a high-performance electrode material for supercapacitors, Electrochim. Acta 260 (2018) 952–958, https://doi.org/10.1016/j.electacta.2017.12.074.

[6] S. Senobari, A. Nezamzadeh-Ejhieh, A comprehensive study on the enhanced photocatalytic activity of CuO-NiO nanoparticles: designing the experiments, J. Mol. Liq. 261 (2018) 208–217, https://doi.org/10.1016/j.molliq.2018.04.028.

[7] S. Mørup, D.E. Madsen, C. Frandsen, C.R.H. Bahl, M.F. Hansen, Experimental and theoretical studies of nanoparticles of antiferromagnetic materials, J. Phys. Condens. Matter 19 (2007) 213202, https://doi.org/10.1088/0953-8984/19/21/213202.

[8] A.V. Ushakov, I.V. Karpov, A.A. Lepeshev, Peculiarities of magnetic behavior of CuO nanoparticles produced by plasma-arc synthesis in a wide temperature range, J. Supercond. Nov. Magnetism 30 (12) (2017) 3351–3354, https://doi.org/10.1007/s10948-017-4311-2.

[9] A.A. Lepeshev, I.V. Karpov, A.V. Ushakov, Production of high-coercivity materials based on BaFe12O19 by crystallization of plasma-sputtered powders, Mat. Res. Exp. 4 (11) (2017) 116107, https://doi.org/10.1088/2053-1591/aa98ac.

[10] E. Winkler, R.D. Zysler, M. Vasquez Mansilla, D. Fiorani, Surface anisotropy effects in NiO nanoparticles, Phys. Rev. B 72 (2005) 132409, https://doi.org/10.1103/PhysRevB.72.132409.

[11] M. Tadić, M. Panjan, D. Marković, I. Milošević, V. Spasojević, Unusual magnetic properties of NiO nanoparticles embedded in a silica matrix, J. Alloys Compd. 509 (25) (2011) 7134–7138, https://doi.org/10.1016/j.jallcom.2011.04.032.

[12] S.D. Tiwari, K.P. Rajeev, Signatures of spin-glass freezing in NiO nanoparticles, Phys. Rev. B 72 (2005) 104433, https://doi.org/10.1103/PhysRevB.72.104433.

[13] M. Tadic, D. Nikolic, M. Panjan, G.R. Blake, Magnetic properties of NiO (nickel oxide) nanoparticles: blocking temperature and Neel temperature, J. Alloys Compd. 647 (2015) 1061–1068, https://doi.org/10.1016/j.jallcom.2015.06.027.

[14] K. Fominykh, J.M. Feckl, J. Sicklinger, M. Döblinger, S. Böcklein, J. Ziegler, L. Peter, J. Rathousky, E.-W. Scheidt, T. Bein, D. Fattakhova-Rohlfing, Ultrasmall dispersible crystalline nickel oxide nanoparticles as high-performance catalysts for electrochemical water splitting, Adv. Funct. Mat. 24 (21) (2014) 3123–3129, https://doi.org/10.1002/adfm.201303600.

[15] B. Sasi, K.G. Gopchandran, Nanostructured mesoporous nickel oxide thin films, Nanotechnology 18 (11) (2007) 115613, https://doi.org/10.1088/0957-4484/18/11/115613.

[16] G. Cai, X. Wang, M. Cui, P. Darmawan, J. Wang, A.L.-S. Eh, P.S. Lee, Electrochromo-supercapacitor based on direct growth of NiO nanoparticles, Nano Energy 12 (2015) 258–267, https://doi.org/10.1016/j.nanoen.2014.12.031.

[17] J.R.A. Sietsma, J.D. Meeldijk, J.P. Den Breejen, M. Versluijs-Helder, A.J. Van Dillen, P.E. De Jongh, K.P. De Jong, The preparation of supported NiO and Co_3O_4 nanoparticles by the nitric oxide controlled thermal decomposition of nitrates, Angew. Chem. Int. Ed. 46 (24) (2007) 4547–4549, https://doi.org/10.1002/anie.200700608.

[18] B. Lu, X.L. Dong, H. Huang, X.F. Zhang, X.G. Zhu, J.P. Lei, J.P. Sun, Microwave absorption properties of the core/shell-type iron and nickel nanoparticles, J. Magn. Magn Mater. 320 (6) (2008) 1106–1111, https://doi.org/10.1016/j.jmmm.2007.10.030.

[19] A.C. Johnston-Peck, J. Wang, J.B. Tracy, Synthesis and structural and magnetic characterization of Ni(Core)/NiO(Shell) nanoparticles, ACS Nano 3 (5) (2009) 1077–1084, https://doi.org/10.1021/nn900019x.

[20] I.V. Karpov, A.V. Ushakov, A.A. Lepeshev, L.Yu Fedorov, Plasma-chemical reactor based on a low-pressure pulsed arc discharge for synthesis of nanopowders, Tech. Phys. 62 (1) (2017) 168–173, https://doi.org/10.1134/S106378421701011X.

[21] A.V. Ushakov, I.V. Karpov, A.A. Lepeshev, Influence of the oxygen concentration on the formation of crystalline phases of TiO_2 during the low-pressure arc-discharge, Plasma Synth. Tech. Phys. 61 (2) (2016) 260–264, https://doi.org/10.1134/S1063784216020262.

[22] A.A. Lepeshev, O.A. Bayukov, E.A. Rozhkova, I.V. Karpov, A.V. Ushakov, L. Yu Fedorov, Modification of the phase composition and structure of the quasicrystalline Al-Cu-Fe alloy prepared by plasma spraying, Phys. Solid State 57 (2) (2015) 255–259, https://doi.org/10.1134/S1063783415020249.

[23] A.A. Lepeshev, A.V. Ushakov, I.V. Karpov, D.A. Balaev, A.A. Krasikov, A. A. Dubrovskiy, D.A. Velikanov, M.I. Petrov, Particularities of the magnetic state of CuO nanoparticles produced by low-pressure plasma arc discharge, J. Supercond. Nov. Magnetism 30 (4) (2017) 931–936, https://doi.org/10.1007/s10948-016-3885-4.

[24] J. Tauc, Optical Properties of Solids, Academic Press Inc, New York, 1966, p. 155.

[25] M. Alagiri, S. Ponnusamy, C. Muthamizhchelvan, Synthesis and characterization of NiO nanoparticles by sol–gel method, J. Mater. Sci. Mater. Electron. 23 (3) (2012) 728–732, https://doi.org/10.1007/s10854-011-0479-6.

[26] M.S. Seehra, V.S. Babu, A. Manivannan, J.W. Lynn, Neutron scattering and magnetic studies of ferrihydrite nanoparticles, Phys. Rev. B 61 (5) (2000) 3513, https://doi.org/10.1103/PhysRevB.61.3513.

[27] R. Bhowmik, R. Nagarajan, R. Ranganathan, Magnetic enhancement in antiferromagnetic nanoparticle of $CoRh_2O_4$, Phys. Rev. B 69 (5) (2004), 054430, https://doi.org/10.1103/PhysRevB.69.054430.

[28] E. Winkler, R.D. Zysler, M.V. Mansilla, D. Fiorani, D. Rinaldi, M. Vasilakaki, K. N. Trohidou, Surface spin-glass freezing in interacting core–shell NiO nanoparticles, Nanotechnology 19 (2008) 185702, https://doi.org/10.1088/0957-4484/19/18/185702.

[29] I.V. Karpov, A.V. Ushakov, V.G. Demin, A.A. Shaihadinov, A.I. Demchenko, L. Yu Fedorov, E.A. Goncharova, A.K. Abkaryan, Investigation of the residual stresses effect on the magnetic properties of CuO nanoparticles synthesized in a low-pressure arc discharge plasma, J. Magn. Magn. Mater. 490 (2019) 165492, https://doi.org/10.1016/j.jmmm.2019.165492.

[30] A.-L. Adenot, S. Deprot, F. Bertin, D. Bois, O. Acher, Magneto-elastic anisotropy of ferromagnetic glass-coated microwires, J. Magn. Magn. Mater. 272–276 (2004) E1115–E1116, https://doi.org/10.1016/j.jmmm.2003.12.125.

[31] M. Wuttig, X. Liu, Ultrathin Metal Films: Magnetic and Structural Properties, Springer-Verlag, Germany, 2004, p. 376.